Shortcuts to Adiabaticity in Digitized Adiabatic Quantum Computing

Narendra N. Hegade,[1] Koushik Paul,[1,*] Yongcheng Ding,[1,2] Mikel Sanz,[2,3,4] F. Albarrán-Arriagada,[1] Enrique Solano,[1,2,3,4] and Xi Chen[1,2,†]

[1] *International Center of Quantum Artificial Intelligence for Science and Technology (QuArtist) and Department of Physics, Shanghai University, Shanghai 200444, China*

[2] *Department of Physical Chemistry, University of the Basque Country UPV/EHU, Apartado 644, 48080 Bilbao, Spain*

[3] *IKERBASQUE, Basque Foundation for Science, Plaza Euskadi 5, 48009 Bilbao, Spain*

[4] *IQM, Nymphenburgerstr. 86, 80636 Munich, Germany*

(Received 9 September 2020; revised 23 December 2020; accepted 26 January 2021; published 16 February 2021)

Shortcuts to adiabaticity are well-known methods for controlling the quantum dynamics beyond the adiabatic criteria, where counterdiabatic (CD) driving provides a promising means to speed up quantum many-body systems. In this work, we show the applicability of CD driving to enhance the digitized adiabatic quantum computing paradigm in terms of fidelity and total simulation time. We study the state evolution of an Ising spin chain using the digitized version of the standard CD driving and its variants derived from the variational approach. We apply this technique in the preparation of Bell and Greenberger-Horne-Zeilinger states with high fidelity using a very shallow quantum circuit. We implement this proposal on the IBM quantum computer, proving its usefulness for the speed up of adiabatic quantum computing in noisy intermediate-scale quantum devices.

DOI: 10.1103/PhysRevApplied.15.024038

I. INTRODUCTION

Quantum computing is known to have significant advantages in solving certain computational tasks, such as simulating quantum systems [1–5], machine learning [6–9], solving optimization problems [10–12], cryptography [13, 14], and several others. Recent advancements in quantum technologies have already shown that quantum computers can outperform currently existing classical computers [15].

Quantum adiabatic algorithms (QAAs) [16–19] are one of the leading candidates for solving optimization problems [20–22]. In adiabatic quantum computation (AQC), we start with a simple Hamiltonian whose ground state can be easily prepared and evolve the system adiabatically to the ground state of the final Hamiltonian, which encodes the solution of the optimization problem. This is embodied by the well-known method of quantum annealing [23]. Quantum annealers, such as the D-Wave machine [24], provide the testbed for adiabatic algorithms [25]. Despite its applications, quantum annealers have certain limitations, such as difficulty in implementing nonstoquastic Hamiltonian, limited qubit connectivity, and noise. Although AQC is equivalent to the standard circuit model [26], the advantage of digital quantum computation over quantum annealers is that the circuit model offers more flexibility to construct arbitrary interactions, and it is consistent with error correction. The recent work of Barends *et al.* [27] combines the advantage of AQC and the circuit model, termed digitized adiabatic quantum computation (DAQC), has been presented and implemented on a superconducting system.

QAAs are generally governed by the quantum adiabatic theorem that restricts a system to evolve along a specific eigenstate, i.e., from the ground state of an initial Hamiltonian $\hat{H}_i$ to the ground state of a final Hamiltonian $\hat{H}_f$, while the evolution is considerably slow. The computation time for the QAA depends on the minimum energy gap between the successive eigenstates during the evolution. When the system size increases, this poses a significant disadvantage for the implementation of the QAA as the energy gap decreases with increasing system size, which ends up in transition between various instantaneous eigenstates. One has to increase the adiabatic evolution time to circumvent such an issue. However, in practice, evolution time for the QAA is significantly larger than the coherence time of current quantum computers, leading to the loss of fidelity of the evolution.

The techniques of "shortcuts to adiabaticity" (STA) [28,29] have been developed during the past decade and proved to be extremely useful for accelerating quantum adiabatic processes in general [30]. Various techniques like

*koushikpal09@gmail.com
†xchen@shu.edu.cn

 © 2021 American Physical Society

counterdiabatic (CD) driving (equivalently transitionless quantum algorithm) [31–33], invariant-based inverse engineering [34,35], and fast-forward scaling [36,37] are rigorously explored and experimentally implemented in several physical setups [38–40]. Among these works, studies dedicated to Ising and Heisenberg spin models are of particular interest due to their relevance to the applicability and implementation of modern-day quantum algorithms [41]. Here we concentrate on the CD driving approach for applying STA, which has been especially useful for studying fast dynamics [42–46], preparation of entangled states [47–50], quantum annealing [51–53], etc. Nevertheless, the theoretical formulation of the conventional CD driving requires knowledge of the eigenspectrum corresponding to the system Hamiltonian, which poses a formidable challenge to obtain the exact CD driving, particularly in the case of a many-body system. The way out is to use numerical optimization methods [54–56] for obtaining the approximate CD coefficients that improve the fidelity.

In this work, we propose a method to achieve DAQC with a shallow quantum circuit. In order to achieve fast evolution without any unwanted nondiabatic transition, we use an auxiliary CD term along with the original Hamiltonian. Starting with Berry's transitionless quantum driving for a single-spin system, we opt to calculate local auxiliary interactions for a weakly interacting many-spin system. Because of the difficulties in calculation and implementation of the exact CD driving for a many-body system using the method of Ref. [33], we use the recently proposed variational method for computing the approximate CD terms [57,58]. To check this technique's validity and performance, we study a nonintegrable Ising spin model with variational local CD driving and state preparation of the N-qubit Greenberger-Horne-Zeilinger (GHZ) state.

The paper is organized as follows. In Sec. II, we give a detailed insight into the implementation of STA in a single spin, where the CD interaction can be exactly calculated using Berry's formula. In Sec. III we explain the application of the approximate local CD driving and its limitations when applied to strongly interacting many-spin systems. In Sec. IV, we show the improvement in fidelity when the approximate CD driving is calculated using the nested commutator (NC) through the adiabatic gauge potential using the variational approach. This is followed by an example of entangled state preparation, where we show the preparation of the Bell state and GHZ state for few spin systems with high fidelity. Finally, in Sec. V we summarize our findings and discuss the scope for future research.

II. SINGLE-SPIN SYSTEM

We begin our heuristic discussions with a single spin in the presence of a time-dependent external magnetic field $\mathbf{h}(t)$, represented by a two-level Hamiltonian given by

$$\hat{H}_0^{(1)}(t) = \mathbf{h}(t)\cdot\hat{\boldsymbol{\sigma}}, \tag{1}$$

where $\hat{\boldsymbol{\sigma}}$ represents the Pauli matrices and the superscript "(1)" represents the number of spins. Following the general method for AQC, also that of quantum annealing, we express this Hamiltonian as a combination of two time-independent parts.

$$\hat{H}_0^{(1)}(t) = [1-\lambda(t)]\hat{H}_i + \lambda(t)\hat{H}_f, \tag{2}$$

where $\hat{H}_i$ and $\hat{H}_f$ are time independent with ground states $|\psi_i\rangle$ and $|\psi_f\rangle$, respectively. The time dependence of the system is introduced through the parameter $\lambda(t)$. The initial Hamiltonian is chosen as $\hat{H}_i = h_x\sigma_x$ and the final Hamiltonian as $\hat{H}_f = h_z\sigma_z$, where h_x and h_z are the magnetic field strengths along the respective directions. Such a choice leads one to express the magnetic field effectively as $\mathbf{h}(t) = [h_x\{1-\lambda(t)\}, 0, h_z\lambda(t)]^\top$. AQC, in its rudimentary approach, allows $\lambda(t)$ to be any function that varies from 0 to 1 and drives the system from $|\psi_i\rangle$ to $|\psi_f\rangle$. Although the most general way to choose it is as a linear function, here, to begin with, it is considered as $\lambda(t) = \sin^2(\omega t)$, where $\omega = \pi/2T$ with T being the total evolution time. Although $\hat{H}_0(t)$ is extremely elementary and can easily be implemented in the circuit model [59], there are hints that the evolution can be improved significantly using the STA [43]. In this case, one should be tempted to find out the CD term, which is somewhat straightforward to calculate using [33]

$$\hat{H}_{\rm CD}^{(1)}(t) = \frac{1}{2|\mathbf{h}(t)|^2}[\mathbf{h}(t)\times\dot{\mathbf{h}}(t)]\cdot\hat{\boldsymbol{\sigma}}, \tag{3}$$

yielding the explicit form as

$$\hat{H}_{\rm CD}^{(1)}(t) = F^{(1)}(t)\sigma_y = -\frac{1}{2}\frac{h_x h_z \partial_t[1-\lambda(t)]}{h_x^2[1-\lambda(t)]^2 + h_z^2\lambda^2(t)}\sigma_y. \tag{4}$$

Therefore, the total Hamiltonian assisted with the CD term becomes

$$\hat{H}^{(1)}(t) = [1-\lambda(t)]h_x\sigma_x + \lambda(t)h_z\sigma_z + F^{(1)}(t)\sigma_y. \tag{5}$$

Note that the introduction of the CD term should not affect the initial and final states, since $F^{(1)}(t)$ should always satisfy the boundary conditions $F^{(1)}(t=0) = F^{(1)}(t=T) = 0$. Also, the STA methods generally follow the inverse engineering approach of quantum control, i.e., designing the interaction for achieving the desired eigenstates. Therefore, the notion of the eigenstate, although not that essential in traditional AQC, turns out to be extremely important in the present case. Here, the initial state of

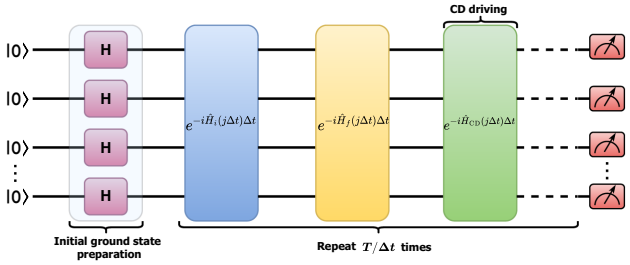

FIG. 1. Circuit implementation for the digitized adiabatic evolution using CD driving, where T is the total evolution time and Δt is the step size. Initial state is prepared by applying Hadamard gate (H) on each qubit. The circuit is repeated $n = T/\Delta t$ times, where the Hamiltonians satisfy the condition $\hat{H}_f(0) = \hat{H}_{\rm CD}(0) = \hat{H}_{\rm CD}(T) = \hat{H}_i(T) = 0$.

$\hat{H}_i$ is chosen in the computational basis, i.e., $\{|0\rangle, |1\rangle\}$, as $|\psi_i\rangle = |+\rangle$ and the final state is $|\psi_f\rangle = |1\rangle$. It should be noted that $|+\rangle = (|0\rangle + |1\rangle)/\sqrt{2}$ and $|1\rangle$ are the natural ground states of $\hat{H}_i$ and $\hat{H}_f$, respectively, but these choices are not restricted to the ground states only. However, such a choice restraints the qubit in the ground state, minimizing the effect of the decoherences.

To implement the evolution using one qubit, we use the first-order Trotter-Suzuki formula. The time evolution is digitized with n small time steps Δt [see Eq. (A3)]. Ideally, the discretized version of AQC approaches the actual adiabatic evolution for $n = T/\Delta t \to \infty$ ($\Delta t \to 0$). Although, in real situations, n is finite and it has to be a relatively small number since each trotter step is being implemented by three rotation gates (see Appendix A). The error associated with the first-order trotterization is $\mathcal{O}(\Delta t^2)$ [60]. The general circuit for implementing the evolution using CD driving is shown in Fig. 1.

To perform the simulation, we use the publicly available five-qubit superconducting quantum computer of IBM Quantum Experience [61]. For the single-spin experiment, we use qubit Q_0 on *ibmq_essex*. Since the single-qubit gate error of the device is of the order of 10^{-4}, the initial state is prepared with very high fidelity. Also, a significant error in this simulation comes from the readout error (approximately 4%); for that, we use the error mitigation technique using the matrix inversion method described in Appendix C.

In the simulation, time evolution takes place between $|+\rangle$ to $|1\rangle$ and is measured in the computational basis, which restricts the variation of the probability between 0.5 to 1; see Fig. 2. Since the trotter error is of the order $\mathcal{O}(\Delta t^2)$, we choose $\Delta t = 0.2$ and $T = 1$ for the comparison of the evolution using DAQC and STA-assisted DAQC. To study the probability of the final ground state $P_{\rm g.s.} = |\langle\psi(t)|1\rangle|^2$, where $|\psi(t)\rangle$ denotes the time-evolved state of $\hat{H}_0(t)$, measurement is performed at each progressing time step. For sampling, we repeat each circuit many

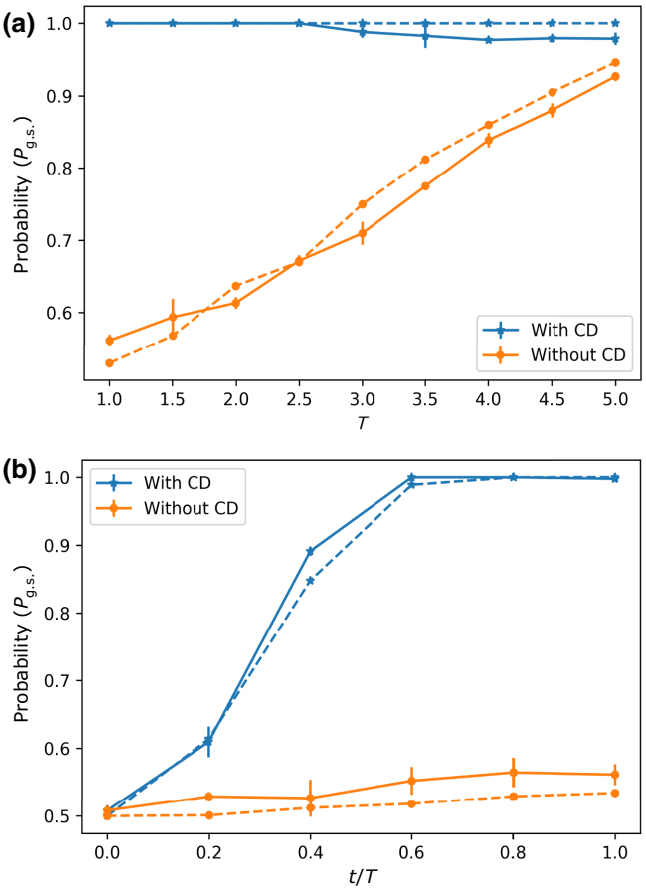

FIG. 2. (a) The final ground state probability $P_{\rm g.s.}$ versus the simulation time for a single qubit using CD driving on the `ibmq_essex` quantum computer (solid blue line) compared to the ideal simulator (dashed blue line). The simulation without CD driving in the real device (solid orange line) and ideal simulator (dotted orange line). (b) Time evolution using DAQC and STA methods for $T = 1$. The parameters are as follows: $\Delta t = 0.2$, $h_x = -1$, $h_z = 1$, and the number of shots ($N_{\rm shots}$) $= 1024$.

times, and the number of repetitions is denoted by $N_{\rm shots}$. In Fig. 2(b) we show a single evolution of the qubit governed by both Eqs. (2) and (5), using both simulation and experiment on a real quantum device. With the application of CD driving $F^{(1)}(t)$, the probability of getting state $|1\rangle$ from the experiment comes out to be around 0.997. Whereas, when the CD driving is zero, i.e., for the adiabatic evolution, the final state probability is around 0.561 only. However, if the evolution is extended for a larger T, we could obtain a much higher probability, even without $F^{(1)}(t)$, a signature of the typical adiabatic process. This is evident in Fig. 2(a), where the fidelity of the evolution (in the computational basis) for different T is shown. Even when $T = 1$ ($\Delta t = 0.2$) using the STA method, the final ground state is reached with nearly unit fidelity. We observe that fidelity for the STA method for large T maintains its value at around 0.978. However, for the

adiabatic case, fidelity gradually increases with increasing simulation time and the average fidelity will be around 0.927 for $T = 5$. Note that in Fig. 2(a) the experimental values differ slightly from the exact simulation values, and the difference is slightly larger for the STA-assisted case. As T increases, the circuit depth becomes larger, which results in ramping up of the gate errors, affecting STA more than the adiabatic case as it requires more gates for implementation.

III. LOCAL COUNTERDIABATIC DRIVING

The results in Sec. II establish the fact that STA-assisted DAQC shows significant improvement over the DAQC, at least when a single qubit is considered. However, such implementation becomes far more interesting when multiple qubits are considered. The simplest choice is a system of N interacting spins in a one-dimensional lattice, coupled by a time-dependent exchange interaction $J(t)$ with a rotating magnetic field acting upon it. Here we consider $J(t)$ to constitute $\sigma_z\sigma_z$-type interaction with J_0 being the coupling amplitude. The spins are initially aligned along the transverse magnetic field h_x, while an Ising Hamiltonian represents the system's final state. The total Hamiltonian is represented as

$$\hat{H}_0^{(N)}(t) = [1-\lambda(t)]\sum_{j=1}^{N} h_x\sigma_x^j + \lambda(t)\sum_{j=1}^{N}(h_z^j\sigma_z^j + J_0\sigma_z^j\sigma_z^{j+1}), \tag{6}$$

where the scheduling $\lambda(t) = \sin^2[(\pi/2)\sin^2(\pi t/2T)]$ is chosen. Note that, similar to the magnetic field components, the time dependence of the exchange interaction is also expressed through the scheduling $\lambda(t)$, i.e., $J(t) = J_0\lambda(t)$. The traditional approaches to finding the CD driving are predominantly limited to two- and three-level systems and become more complex for higher-dimensional many-body systems. However, for interacting many spin systems, as in the preceding section, a local CD driving could be more useful. Instead of acting on the whole system, a set of approximated interactions could be designed to control the spins individually. Such a type of local CD driving is more general and can be extended to a larger number of spins.

A. Local CD term from Berry's algorithm

To realize such CD driving, it is intuitive to approximate the system as a noninteracting system. Using the mean-field approximation, this can be achieved effectively for an infinite-range Ising model [62]. However, this is problematic for DAQC, as it requires self-consistent feedback $\langle\sigma_j\rangle$ after every step. Instead, we consider a more direct approach. Since, at $t = 0$, the spins have no mutual interaction and are dictated by the transverse magnetic field, it can be assumed that, during the evolution, the magnitudes of h_z^j and J_0 grow gradually from zero to some maximum value while the system evolves gradually from $\hat{H}_i$ to $\hat{H}_f$. Therefore, we approximate that those spins are governed by a local effective magnetic field, given by $h(t) = [h_x\{1-\lambda(t)\}, 0, \tilde{h}_z^j\lambda(t)]^\top$, where $\tilde{h}_z^j = h_z^j + J_0$. Subsequently, the local CD driving is calculated and summed over for each spin using Eq. (3),

$$\begin{aligned}\hat{H}_{\rm CD}^{(N)}(t) &= \sum_{j=1}^{N} F_j^{(N)}(t)\sigma_y^j \\ &= \sum_{j=1}^{N} \frac{-h_x\tilde{h}_z^j\partial_t[1-\lambda(t)]}{2\{h_x^2[1-\lambda(t)]^2 + (\tilde{h}_z^j)^2\lambda^2(t)\}}\sigma_y^j. \end{aligned} \tag{7}$$

Therefore, the modified Hamiltonian that governs the evolution can be expressed as

$$\hat{H}^{(N)}(t) = \hat{H}_0^{(N)}(t) + \sum_{j=1}^{N} F_j^{(N)}(t)\sigma_y^j. \tag{8}$$

As an example, we consider the interacting two-qubit system, where the time evolution for $\hat{H}^{(2)}(t)$ can be easily implemented by two-qubit entangling gates and single-qubit rotation gates. The initial and target states chosen for the evolution are $|{+}{+}\rangle$ and $|11\rangle$, respectively, which are inferred directly from the parameters $h_x = -1$, $h_z^1 = h_z^2 = 1$, and $J_0 = -0.1$. The time evolutions for STA-assisted DAQC and DAQC for two qubits are shown in Fig. 3. Again, like the single-qubit case, one can achieve a high fidelity for the target state preparation. The result obtained from the ideal digital simulator, in Fig. 3(a), shows that, when the additional term $\hat{F}_j^{(2)}(t)$ is considered, the target state can be achieved with almost unit fidelity. Furthermore, when a single evolution is considered, as depicted in Fig. 3(b), the target state can be achieved substantially faster than adiabatic evolution. However, when implemented in the real experiment, a fidelity around 0.93 is achieved with the application of the CD term, where the fidelity in the computational basis is calculated as $|\langle\psi_i(n\Delta t)|\psi_f\rangle|^2$. The application of the CD term is more suitable when the evolution time T is small. In principle, the fidelity should remain the same even if we increase the number of time steps. Nevertheless, due to limited coherence time and the increasing number of gates required to implement the CD term, fidelity gradually decreases, as depicted in Fig. 3(a).

B. Local CD term from the variational approach

A recently proposed method by Sels and Polkovnikov [57], based on the variational approach, also provides an alternative to calculate the approximate CD Hamiltonian with only local terms. The method for this calculation is

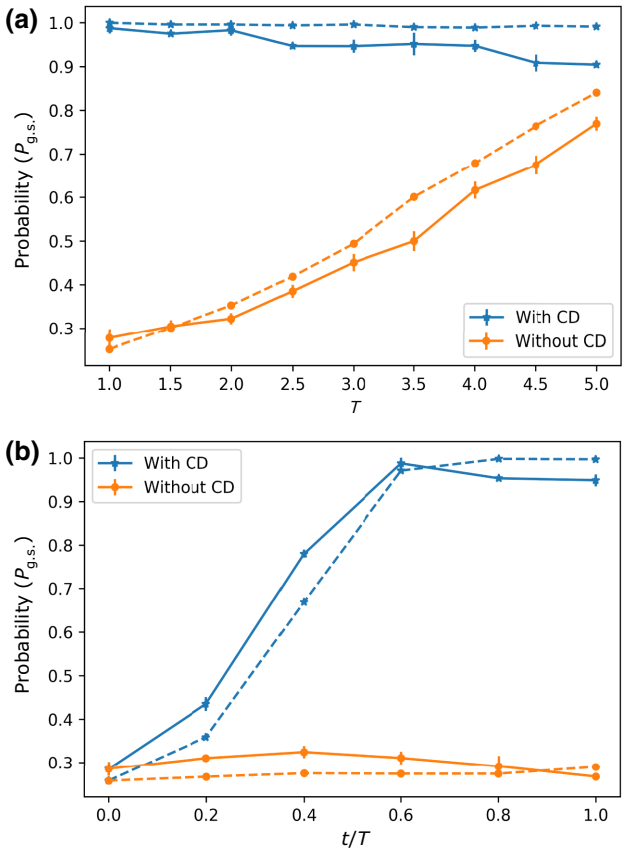

FIG. 3. (a) The final ground state probability $P_{\text{g.s.}}$ versus the simulation time for the two interacting spin systems ($\Delta t = 0.5$). The orange solid curve represents the time evolution using the STA method, the solid blue curve represents the DAQC on the `ibmq_london` five-qubit quantum processor. As the evolution time increases, the gate error starts to dominate, which is clearly inferred from the figure. (b) Implementation of the time evolution for the two-spin system without the CD term (solid orange line) and including the CD term (solid blue line). The dotted lines correspond to the result from the ideal simulator. The parameters are as follows: simulation time $T = 1$, $\Delta t = 0.2$, $h_x = -1, h_z^1 = h_z^2 = 1$, $J_0 = -0.1$, and $N_{\text{shots}} = 1024$. Both the curves show expected profiles.

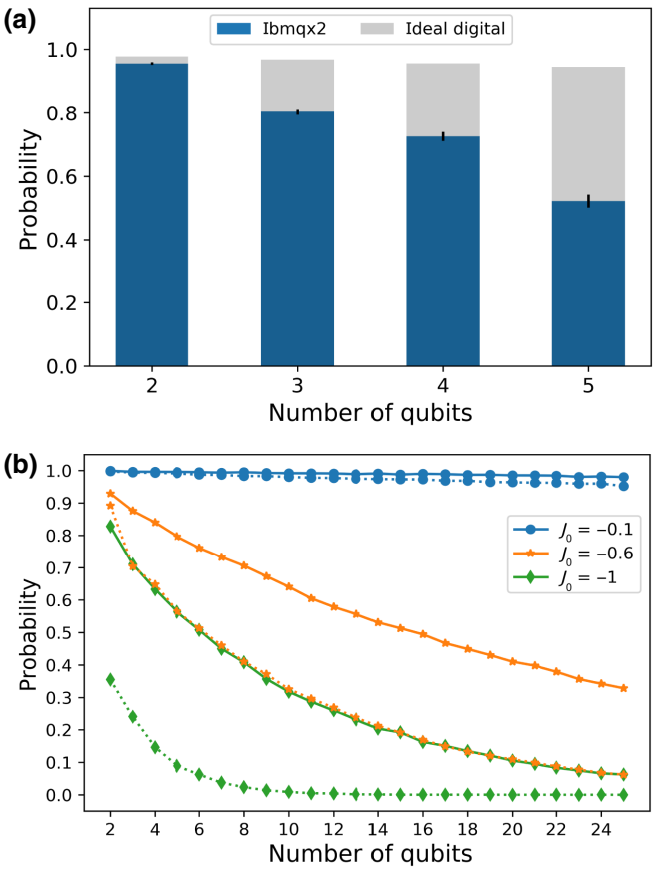

FIG. 4. (a) For the nonintegrable Ising model, the probability of obtaining the final ground state using the local CD term calculated via the variational method for up to a five-qubit system is depicted. The experiment is performed on the five-qubit `ibmqx2` processor. The experimental parameters are $J_0 = -0.1$, $h_x = -1$, $h_z^j = 1$, $N_{\text{shots}} = 8192$. (b) The probability of obtaining the final ground state as a function of the coupling strength using local CD driving for up to 25 qubits. The solid line is for the local CD term from the variational approach, and the dotted line is for the local CD term from Berry's formula; see Eq. (7). The parameters chosen are $h_x = -1$, $h_z^j = 1$, $dt = 0.1$, and $T = 1$. The simulation is performed with the `qasm_simulator`.

to choose an appropriate adiabatic gauge potential $\hat{A}_\lambda^*$ [63] and minimize the action $S = \text{Tr}[\hat{G}_\lambda^2]$, where the operator $\hat{G}_\lambda$ is defined by $\hat{G}_\lambda = \partial_\lambda \hat{H} + i[\hat{A}_\lambda^*, \hat{H}]$ (see Appendix B). The CD driving using this method is expressed as $\hat{H}_{\text{CD}}^{(N)} = \dot{\lambda}\hat{A}_\lambda^*$. Since the Hamiltonian contains only real values in the z basis, the simplest ansatz is to choose $\hat{A}_\lambda^* = \sum_j \alpha_j(t)\sigma_y^j$, i.e., applying an additional magnetic field along the y direction for each spin. By minimizing the action S with respect to α_j, the variational coefficient $\alpha_j(t)$ is analytically calculated, which takes the general form, for Eq. (6) [57],

$$\alpha_j(t) = \frac{1}{2}\frac{h_x h_z^j}{h_x^2[1-\lambda(t)]^2 + (h_z^j + 2J_0)^2\lambda^2(t)}. \tag{9}$$

The expression for $\hat{H}_{\text{CD}}^{(N)} = \sum_j \dot{\lambda}\alpha_j(t)\sigma_y^j$ is similar to that of Eq. (7) except for a few modifications. In Fig. 4(a), the probabilities of obtaining the ground state, from both the ideal simulator and the experimentally implemented data from `ibmqx2`, are shown for up to five qubits. Like the previous case, the final ground state $|11\ldots1\rangle$ can be prepared using the additional $\hat{H}_{\text{CD}}^{(N)}$ with high fidelity. The ideal simulator data show that the final probability, $|\langle\psi(T)|11\ldots1\rangle|^2$ reaches almost unity for $T = 1$ in five trotter steps, especially when $|J_0|$ is small. However, with increasing system size, the required number of controlled NOT (CNOT) gates increases, where each CNOT introduces, on average, 2% error on `ibmqx2`, which reduces the success probability.

It should be noted that, in the above discussion, the interaction strength $|J_0|$ is kept sufficiently small compared to the external magnetic field, $|J_0| \ll h_z^j$. The ground state of the final Hamiltonian is a ferromagnetic state, i.e., either $|00\ldots0\rangle$ or $|11\ldots1\rangle$, depending on the sign of h_z^j. In such a scenario, the evolution assisted by the local CD terms in Eqs. (7) and (9) produces the exact final ground state. In Fig. 4(b) we compare the probability of the interacting multiqubit system with ground state $|111\ldots1\rangle$. For $|J_0| \ll h_z^j$, the probability is around 98% in the ideal simulator for both the methods. One can observe that the success probability is almost independent of the system size. The probability starts to decrease gradually with increasing N when we increase J_0. For $|J_0| \sim h_z^j/2$, the final state probability decreases linearly with increasing N. Also, when the interaction strength becomes comparable to the magnetic field, i.e., $|J_0| \sim h_z^j$, an exponential decay in the probability can be observed with increasing system size. Apparently, when J_0 becomes large, the probability using Eq. (4) decreases drastically and reduces to 35%, even for two qubits. Whereas, for the variational approach, the probability is significantly higher for large $|J_0|$ values. When the ground state is degenerate, the obtained result seems to differ from the actual ground state. For instance, when $J_0 = 2$, with similar values for the other parameters, the ground state becomes doubly degenerate, i.e., the states $|01\rangle$ and $|10\rangle$, the inclusion of the local CD term fails to produce this state. This turns out to be true for many spin systems also. In fact, the calculation of the local CD term is based on the approximation that every spin is treated individually by considering an effective magnetic field acting upon each spin. The effects of interaction $|J_0|$ are undermined while calculating the CD term. As a result, when $|J_0|$ is comparable or stronger than that of the local magnetic field, the CD term hinders the evolution of the system into the exact ground state.

Subsequently, when $h_z^j = 0$, the final ground state becomes entangled, and one can deduce from Eq. (7) that, for small $|J_0|$, the CD term becomes small, i.e., $\hat{F}_j^{(N)}(t) \to 0$. In such cases, the final evolved state, for a short simulation time T, does not match the adiabatic one. For the variational approach, the CD term vanishes altogether and cannot be applied using such form. Therefore, if we are to prepare a highly entangled state, the single-qubit approximation for the CD term is not a good choice. This drawback occurs as CD driving is calculated using the σ_y terms, which refers to driving a single qubit with the external magnetic field only. In fact, the spin-spin interaction term decides the final state here and the driving for $\sigma_z\sigma_z$ coupling has to be incorporated. This enforces the fact that the direct approach from the first principle to find the local CD driving is not realistic and should contain other interactions such as $\sigma_y\sigma_z$ and $\sigma_z\sigma_x$, etc. [51].

IV. APPROXIMATE COUNTERDIABATIC DRIVING

Following the discussion in the preceding section, when complex many-body systems are considered, the calculation of the exact CD term becomes difficult. Also, the form of the CD term can be severely complicated with different nonlocal and many-body interaction terms. Besides, it becomes rather difficult to implement systems with such interactions on current quantum computers. Although the local terms, see Eq. (9), from the variational approach give an optimal solution, it is not that useful for preparing entangled states, especially when $h_z^j = 0$. The nature of the CD term from the variational calculation depends on the choice of appropriate adiabatic gauge potential $\hat{A}_\lambda^*$. A recently proposed method gives a more general way to choose the gauge potential by using the NC [58]

$$\hat{A}_\lambda^{(l)} = i\sum_{k=1}^{l} \alpha_k(t)\, \underbrace{\{\hat{H}, [\hat{H}, \ldots, (\hat{H}}_{2k-1}, \partial_\lambda \hat{H})]\}, \tag{10}$$

where l determines the order of the expansion. Depending on the required accuracy, we can keep the number of variational coefficients small. If we consider only the first-order term, our ansatz will be $\hat{A}_\lambda^{(1)} = i\alpha_1(t)[\hat{H}, \partial_\lambda \hat{H}]$, and the effective Hamiltonian can be written as

$$\hat{H}_{\text{eff}}(t) = \hat{H}(\lambda) + \dot{\lambda}\hat{A}_\lambda^{(1)}, \tag{11}$$

where $\dot{\lambda}\hat{A}_\lambda^{(1)}$ is the relevant CD term. First, we apply this technique to the nonintegrable Ising spin model, described by the Hamiltonian in Eq. (6). Considering the two-qubit system ($N = 2$), we approximate the CD term using the first-order NC

$$\hat{H}_{\text{CD}}^{(2)} = 2\alpha_1(t)h_x[h_z(\sigma_y^1 + \sigma_y^2) + J_0(\sigma_y^1\sigma_z^2 + \sigma_z^1\sigma_y^2)] \tag{12}$$

with

$$\alpha_1(t) = \frac{1}{4}\frac{h_z^2 + J_0^2}{\lambda^2(h_z^4 J_0^4 + 3h_z^2 J_0^2) + (1-\lambda)^2 h_x^2(h_z^2 + 4J_0^2)} \tag{13}$$

and $h_z^1 = h_z^2 = h_z$ for simplicity. The second-order term ($l = 2$) can give the exact gauge potential [58]. However, for the experimental demonstration, we only consider the first-order term and implement the time evolution on a quantum processor. The circuit implementation for the CD driving is shown in Appendix A. Using this method, the final ground state is achieved with very few trotter steps compared to digitized adiabatic evolution, which drastically reduces the number of gates required as well as the total simulation time. In Fig. 5, we depict the fidelity as a function of the evolution time using the first-order NC

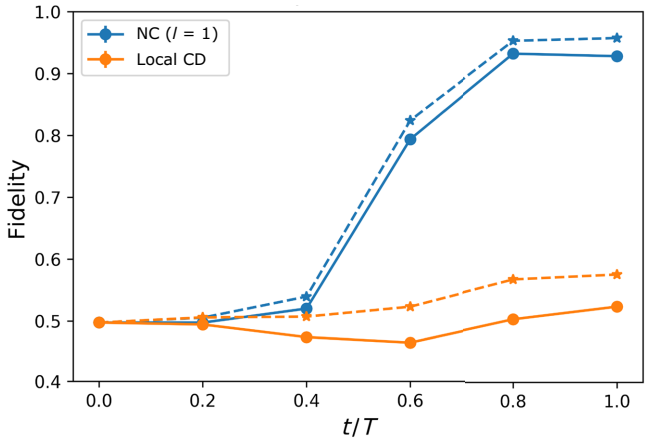

FIG. 5. The fidelity of obtaining the final ground state $(|01\rangle + |10\rangle)/\sqrt{2}$ as a function of the evolution time for local CD and the NC ansatz ($l = 1$) obtained from `ibmq_vigo`. The solid line represents the experimental result and the dashed line represents the result from the ideal digital simulator. The parameters are $J_0 = 2$, $h_z = 0.6$, $T = 1$, $dt = 0.2$, and $N_{\text{shots}} = 8192$.

method when the final ground state is degenerate and compare the result with the local CD term from Eq. (9). The fidelity is much better compared to the local CD case for the degenerate state and thereby it justifies our argument in the preceding section.

Second, we check the reliability and validity as well as the extent of the variational approach in the many-body regime. To this end, we apply this technique to prepare the GHZ state in the Ising spin chain with many spins, described by the Hamiltonian

$$\hat{H}[\lambda(t)] = [1 - \lambda(t)] \sum_j^N h_x \sigma_x^j + \lambda(t) J_0 \sum_j^N \sigma_z^j \sigma_z^{j+1} \quad (14)$$

with N being the number of spins. Here, the periodic boundary condition $\sigma^{N+1} = \sigma^0$ is assumed. Following the variational method described in Sec. 2 and the NC ansatz for the gauge potential in Eq. (10), by considering only the first-order expansion ($l = 1$), we calculate the approximate gauge potential as

$$\hat{A}_\lambda^{(1)} = 2\alpha_1^N(t) J_0 h_x \sum_j^N (\sigma_z^j \sigma_y^{j+1} + \sigma_y^j \sigma_z^{j+1}). \quad (15)$$

The variational coefficient $\alpha_1^N(t)$ is calculated by minimizing the action S. For the experimental demonstration on a quantum processor, we choose a small system with two and three qubits to prepare a Bell state and GHZ state. For the bell state, $(|00\rangle + |11\rangle)/\sqrt{2}$, governed by the Hamiltonian in Eq. (14), the variational coefficient is calculated as $\alpha_1(t) = -\frac{1}{4}[J_0^2\lambda^2 + 4(1-\lambda)^2 h_x^2]$. Here we note that, for two spins, the first-order commutator is proportional to the higher-order terms. The resulting CD driving from the approximate gauge is exact and produces unit fidelity in ideal situations [58]. The same procedure can be followed in the case of more qubits to prepare a GHZ state $|\text{GHZ}\rangle = (|0\rangle^{\otimes N} + |1\rangle^{\otimes N})/\sqrt{2}$ starting from the N-qubit ground state $|+\rangle^{\otimes N}$. Specifically, the variational coefficient for a three-qubit case is given by $\alpha_1(t) = -\frac{1}{2}[5J_0^2\lambda^2 + 8(1-\lambda)^2 h_x^2]$.

The simulation is performed on the five-qubit quantum processor `ibmq_ourense`. A similar trotterization as in Eq. (A5) is used to study the evolution with digitized time step $dt = 0.01$. Using the CD driving with only three trotter steps, the desired bell state is obtained with experimental fidelity 0.984. The ideal digital simulation gives almost unit fidelity ($F = 0.999$). The fidelity is calculated as $F(\rho_1, \rho_2) = \langle\psi_1|\rho_2|\psi_1\rangle$, where the exact bell state is represented by $\rho_1 = |\psi_1\rangle\langle\psi_1|$. Similarly, for the three-qubit system, the ideal digital evolution gives the fidelity 0.935 with the exact GHZ state, and the corresponding experimental fidelity is 0.819. The density matrix representation of the final state (ρ_2) is obtained by performing quantum state tomography for both the Bell and GHZ states and is depicted in Fig. 6. Note that Fig. 7 shows how the fidelity varies with increasing system size on an ideal digital simulator with six trotter steps. The first-order approximation of the CD term provides high fidelity for small system sizes. From the simulation result, we can observe that, for the case of the NC ansatz, there are two regimes (linear and exponential) of the N dependence for a fixed l. For small systems, the lower-order terms in the NC ansatz can significantly suppress the diabatic transitions

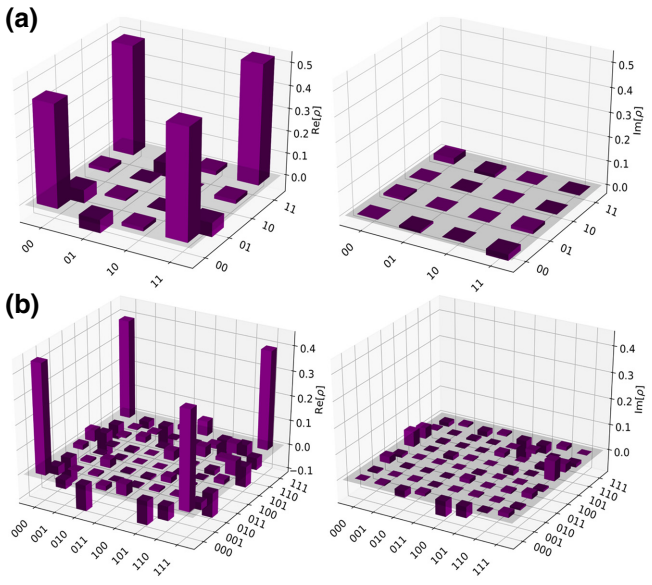

FIG. 6. The density matrix representation of the final ground state obtained from state tomography. (a) The Bell state from `ibmq_ourense` and (b) the GHZ state from `ibmq_vigo`.

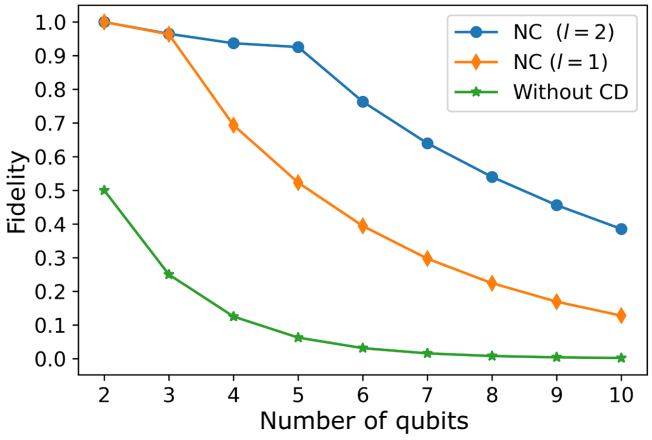

FIG. 7. Fidelity to prepare the GHZ state as a function of system size on an ideal digital simulator with CD term from the NC ansatz with different orders and the naive approach without CD term. The parameters are $T = 0.006$ and $\Delta t = 0.001$.

and give the final state with high fidelity. As the system size increases, the fidelity starts to decay rapidly. However, it still gives a significant improvement over the evolution without the CD term. The variational method tends to provide exact CD driving for larger l values, which, in principle, can give a better fidelity in many-body systems. However, the downside of this method is that, for large l values, the $\hat{A}_\lambda^{(l)}$ can contain many-body nonlocal interaction terms, increasing the gate complexity for the implementation.

V. CONCLUSION

In conclusion, we demonstrate the implementation of digitized STA on a superconducting quantum processor. The problem Hamiltonian, chosen for the simulation, emulates the one-dimensional Ising spin chain. The STA is realized by means of the local and approximate CD driving, which is mainly obtained using two methods: the long-established Berry's algorithm and the recently proposed variational approach. The CD term in our simulation is nonstoquastic in nature; therefore, it cannot be simulated efficiently on a classical computer. The effective Hamiltonian is implemented using the available quantum gates, and the time evolution of the system is studied to achieve the ground state of the problem Hamiltonian. In order to reduce the decoherence effect, we perform circuit optimization and error mitigation. We show that the time steps required to reach the target state are minimal compared to the DAQC method, leading to minimal loss due to the decoherences and accumulated gate errors. In Tables I and II in Appendix B, we compare the total gate counts for each simulation with and without the CD term. For local CD driving, the variational method gives better fidelity for larger systems compared to CD driving calculated from Berry's formula. In general, local CD driving proves to be very effective for weakly interacting spin chains, but when $h_x = 0$ or $h_z^j = 0$ in Eq. (6), both the methods fail to give the desired result. Also, for a strongly interacting spin system, local CD driving gives poor results when the final ground state becomes degenerate. To remedy this situation, approximate CD driving is useful, which can be calculated using the NC method. Comparison of the final state fidelity clearly demonstrates the superiority of the approximate CD term from the NC method compared to the local CD approach. However, the approximate CD term contains two-body interaction terms that require entanglement between successive qubits, resulting in a significant increase in the computational complexity. Furthermore, we can observe from Table II that the running cost is quantified by total gate counts, by comparing the number of gates required to simulate different systems with and without CD driving. More specifically, there is a lower bound on the number of trotter steps needed to achieve unit fidelity. Also, the magnitude of the CD coefficient, yielding the angle of the rotation of the gate, is inversely proportional to the number of trotter steps, clarifying the trade-off between speed and energy in STA [64–66].

As a future direction, the method we use can be generalized to various systems with increasing complexity. Specifically, many of the combinatorial optimization problems like MaxCut and k-SAT problems can be mapped to finding the ground state of a Hamiltonian with spatially inhomogeneous and k-body interaction terms. The NC ansatz can be efficiently generalized for such a system to obtain better approximate solutions. The recent hybrid quantum-classical algorithms like the variational quantum eigensolver and quantum approximate optimization algorithm (QAOA) [67,68] can also benefit by following this method. CD driving requires introducing a new term to the original Hamiltonian; hence, it requires extra gate operations to realize the CD term. However, realizing other STA techniques combined with deep reinforcement learning [69,70] can be used to further decrease the total gate counts with low energetic cost. Also, it would be interesting to explore some of the recently proposed STA methods for many-body systems [71] on a gate-based quantum computer.

This work provides evidence that significant enhancement of the DAQC approach can be achieved using STA methods by decreasing the total computational cost and hence achieving the desired results within the coherence time of the device. This work successfully realizes STA methods in a contemporary superconducting circuit-based quantum computer. Because of the decoherence and gate errors, the time evolution studies are challenging to perform in such devices. Our result provides a beginning to such studies on the speed up of AQC algorithms.

ACKNOWLEDGMENTS

The authors are grateful to Kazutaka Takahashi for useful discussions. We acknowledge support from the National Natural Science Foundation of China (NSFC) (Grant No. 12075145), the STCSM (Grants No. 2019SHZDZX01-ZX04, No. 18010500400, and No. 18ZR1415500), the Program for Eastern Scholar, the Ramón y Cajal program of the Spanish MCIU (RYC-2017-22482), QMiCS (820505) and OpenSuperQ (820363) of the EU Flagship on Quantum Technologies, the Spanish Government under Grant No. PGC2018-095113-B-I00 (MCIU/AEI/FEDER, UE), the Basque Government under Grant No. IT986-16, the EU FET Open Grant Quromorphic (Grant No. 828826), as well as the EPIQUS (Grant No. 899368). This work is also partially supported through HiQ funding for developing QAOA&STA (Grant No. YBN2019115204).

APPENDIX A: METHOD OF DIGITIZATION

The circuit model can efficiently simulate adiabatic quantum computing by using the digitization of continuous adiabatic evolution. The time-dependent Hamiltonians, considered in this work, can be represented as a sum of M k-local terms that act on at most k qubits. This can be represented as

$$\hat{H}(t) = \sum_{m=1}^{M} C_m(t)\hat{H}_m. \tag{A1}$$

The continuous time evolution operator of $\hat{H}(t)$ is given by

$$\hat{U}(0,T) = \mathcal{T}\exp\left[-i\int_0^T dt\hat{H}(t)\right], \tag{A2}$$

where $\mathcal{T}$ is the time ordering operator. The discretization is done using the first-order Trotter-Suzuki formula

$$\hat{U}(0,T) \to \hat{U}(0,T)_{\text{dig}} = \prod_{j=1}^{n}\prod_{m=1}^{M}\exp[-i\Delta t C_m(j\,\Delta t)\hat{H}_m]. \tag{A3}$$

Here the total evolution time T is divided into n equal steps of width Δt, i.e., $n = T/\Delta t$. In this case, the error would be of the order $\mathcal{O}(\Delta t^2)$ [60]. One can also consider a higher-order decomposition, which can give a better approximation by minimizing the error further [72]. However, an interesting observation from our simulation is that the digital adiabatic evolution using CD driving is independent of the simulation time T, and depends only on the number of trotter steps. So, by fixing the total time steps, we can choose an arbitrarily small value for T and Δt so that we can achieve arbitrary precision even with the first-order trotterization. We ignore the time variation of the Hamiltonian $\hat{H}(t)$ on time scales lower than Δt, which contributes an extra error of approximately $\|\partial\hat{H}/\partial t\|\Delta t$ each step. When the Hamiltonian fluctuation is very fast, it is possible to suppress this additional error, which is discussed in Ref. [73]. From Eq. (A3), the digital unitary evolution can be designed for the different Hamiltonians chosen in this work. For instance, one single step of the Trotter-Suzuki decomposition for Eq. (5) will look like

$$\hat{U}(0,\Delta t) = e^{-i\hat{H}(t)\Delta t} \approx e^{-i\theta_x(\Delta t)\sigma_x\Delta t}e^{-i\theta_z(\Delta t)\sigma_z\Delta t}e^{-i\theta_y(\Delta t)\sigma_y\Delta t}, \tag{A4}$$

where $\theta_x(\Delta t) = [1-\lambda(\Delta t)]$, $\theta_z(\Delta t) = \lambda(\Delta t)$, and $\theta_y(\Delta t) = F^{(1)}(\Delta t)$ are the variables that represent the change in the Hamiltonian in each step. Similarly, for Eq. (8), four variables are required for each spin in each step, i.e.,

$$\hat{U}(0,\Delta t) \approx \prod_{j=1}^{2} e^{-i\theta_x(\Delta t)\sigma_x^j\Delta t}e^{-i\theta_z(\Delta t)\sigma_z^j\Delta t}e^{-i\theta_{zz}(\Delta t)\sigma_z^j\sigma_z^{j+1}\Delta t} \times e^{-i\theta_y(\Delta t)\sigma_y^j}. \tag{A5}$$

These unitary operators are implemented in the circuit model. According to the Solovay-Kitaev theorem [74], any k-body unitary operation can be decomposed into a combination of single-qubit and two-qubit gate operations. Some examples of the implementations corresponding to the unitary operators used in this study are as follows.

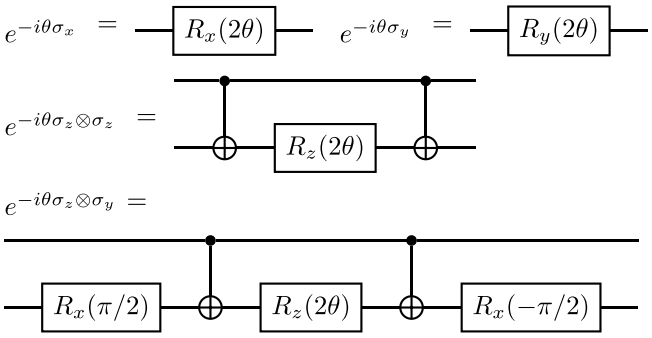

APPENDIX B: APPROXIMATE CD TERM USING THE VARIATIONAL METHOD

The main idea of counterdiabatic driving is to add an auxiliary term to the original Hamiltonian and evolve the system according to an effective Hamiltonian

$$\hat{H}(t) = \hat{H}_0(t) + \dot{\lambda}\hat{A}_\lambda, \tag{B1}$$

where $\hat{H}_0$ is the original Hamiltonian, $\dot{\lambda}$ is the control parameter, and $\hat{A}_\lambda$ is the exact adiabatic gauge potential responsible for the diabatic transitions. For the spin model considered in our simulation, the calculation of

TABLE I. The state fidelity using circuit optimization.

Circuit optimization	Fidelity		Gate count		Expected gate error
	Ideal	Experiment	Rotation	CNOT	
			Bell state preparation		
Optimized	0.999	0.9835	8	2	0.019 27
Not optimized		0.8021	19	14	0.118 34
			GHZ state preparation (three qubits)		
Optimized	0.9325	0.8198	20	7	0.070 63
Not optimized		0.7370	23	15	0.142 76

exact gauge potential results in nonlocal m-body interaction terms. Even though it is possible to implement these interactions using a basic set of quantum gates, the required gates will be huge and increase rapidly with the system size. Instead, for practical purposes, we consider an approximate gauge potential $\hat{A}^*_\lambda$, which satisfies the equation

$$[i\partial_\lambda \hat{H}_0 - (\hat{A}^*_\lambda, \hat{H}_0), \hat{H}_0] = 0. \tag{B2}$$

For the optimal solution, we have to minimize the operator distance between the exact gauge potential and the approximate gauge potential, which is equivalent to minimizing the action

$$S_\lambda(\hat{A}^*_\lambda) = \mathrm{Tr}[\hat{G}^2_\lambda(\hat{A}^*_\lambda)], \tag{B3}$$

where the Hilbert-Schmidt norm $\hat{G}_\lambda$ is given by

$$\hat{G}_\lambda(\hat{A}^*_\lambda) = \partial_\lambda \hat{H}_0 + i[\hat{A}^*_\lambda, \hat{H}_0]. \tag{B4}$$

TABLE II. We compare the number of quantum gates required for the successful implementation of adiabatic evolution on a digital quantum computer by including and excluding the CD term.

System	Trotter step	Rotation gates	CNOT gates	Fidelity
		With CD		
Single-spin system	2	7	⋯	0.995
Nonintegrable Ising model (five qubits, $J_0 = -0.1$)	4	70	40	0.993
Bell state preparation	3	27	14	0.999
GHZ state (three qubits)	4	111	60	0.966
		Without CD		
Single-spin system	20	39	⋯	0.996
Nonintegrable Ising model (five qubits, $J_0 = -0.1$)	30	445	300	0.985
Bell state preparation	24	70	48	0.998
GHZ state (three qubits)	18	105	108	0.962

A simple ansatz for $\hat{A}^*_\lambda$ for the Hamiltonian in Eq. (6) of the main text is $\hat{A}^*_\lambda = \sum_j \alpha_j(t)\sigma^j_y$. This single-qubit approximation works very well even for many-body systems. However, when the spin interaction terms become the leading terms of the adiabatic gauge potential, this ansatz fails. So, we consider a general way to choose the ansatz using a sequence of nested commutators proposed in Ref. [58], that is,

$$\hat{A}^{(l)}_\lambda = i\sum_{k=1}^{l} \alpha_k(t)\, \underbrace{\{\hat{H}, [\hat{H}, \ldots, (\hat{H}}_{2k-1}, \partial_\lambda \hat{H})]\}, \tag{B5}$$

from which, when $l \to \infty$, we get the exact gauge potential.

APPENDIX C: ERROR ANALYSIS

Various errors significantly impact the outcomes of the experiments. The sources of errors can be divided into three main categories. (i) *Discretization error* arises due to the choice of Δt in the trotterization process. (ii) *Cumulative gate error* is a combination of single-qubit gate errors and CNOT errors and increases linearly with the circuit depth. (iii) *Measurement error* arises due to the measurements at the end of the time evolution. Also, if the system evolves for a long time, as in the adiabatic case, the energy relaxation and dephasing also have to be considered. The cross talks between the qubits and other environmental effects can also disturb our simulation, but these effects have not been considered in our simulations.

1. Discretization error

In digital quantum simulation the main source of error arises from the discretization of the continuous-time evolution of a Hamiltonian and decomposing this evolution into a sequence of quantum gates. The discretization can be performed using various methods, but the Trotter-Suzuki (TS) formula is the most widely used method among all because of its simplicity. In our simulation, we consider the first-order TS formula, where the error is of the order $\mathcal{O}(\Delta t^2)$. For a given total time T, we can choose an arbitrarily small value for Δt to decrease the trotter error. However, with small Δt, we need more trotter steps to reach the final time, which will increase the total gate count and eventually lead to accumulation of gate error. One possible solution for this problem is to consider a higher-order TS formula using extra gates [72]. Since the gate error is comparatively larger than the trotter error, we restrict ourselves to a first-order approximation.

2. Gate error

While implementing the time evolution of a system, gate error plays a crucial role. With increasing trotter steps,

the gate error also increases linearly. The average fidelities of a single-qubit and a CNOT gate of the IBM quantum computer in our simulation are 99.95% and 98.5%, respectively. For the experimental implementation on a noisy device, it is necessary to optimize the quantum circuit before sending it to the hardware to get the desired result. In our simulation, to decrease the gate error, we use the transpilation function available in Qiskit Terra for circuit optimization. In Table I we show the experimental fidelities for the preparations of the Bell state and GHZ state with and without circuit optimization. The gate count and the expected gate error are calculated in both cases. In Table II we give the gate counts for the successful implementation of the adiabatic evolution for different systems on a digital quantum computer. From the data, it is conclusive that the inclusion of the CD term can improve fidelity and reduce the total gate count. But the numbers of trotter steps and gates are bounded by the magnitude of the CD term, corresponding to the rotation angle of the gate, thus manifesting the energetic cost of CD driving.

3. Measurement error mitigation

One of the main sources of error in our simulation is the readout error of the device. In the following, we briefly discuss how to mitigate measurement error on a small system using the matrix inversion method. For that, we have to find the response matrix M_R for the given device. To measure M_R, we consider a set of 2^n calibration circuits using only the X gate. Let P_{noisy} be the probability distribution for each of the possible 2^n states obtained from the quantum processor after measuring at the end. Let P_{actual} be the probability distribution without readout noise. Then we can obtain $P_{\text{mitigated}}$, which is approximately equal to P_{actual}, by applying the matrix inversion M_R^{-1} on the obtained result, i.e.,

$$M_R^{-1} P_{\text{noisy}} = P_{\text{mitigated}}. \tag{C1}$$

This method works only when the measurement error is much larger than the single-qubit gate error used for the initial state preparation. This is true for IBMQ devices, where the average single-qubit gate error is of the order of 10^{-4} and the measurement error is of the order of 10^{-2}. In this work we use the tool provided by Qiskit Ignis [75] for performing the measurement error mitigation. More advanced methods can be found in Ref. [76].

[1] Richard P. Feynman, Simulating physics with computers, Int. J. Theor. Phys. **21**, 467 (1999).

[2] Iulia M. Georgescu, Sahel Ashhab, and Franco Nori, Quantum simulation, Rev. Mod. Phys. **86**, 153 (2014).

[3] Andrew A. Houck, Hakan E. Türeci, and Jens Koch, On-chip quantum simulation with superconducting circuits, Nat. Phys. **8**, 292 (2012).

[4] Ben P. Lanyon, Cornelius Hempel, Daniel Nigg, Markus Müller, Rene Gerritsma, F. Zähringer, Philipp Schindler, Julio T Barreiro, Markus Rambach, Gerhard Kirchmair, *et al.*, Universal digital quantum simulation with trapped ions, Science **334**, 57 (2011).

[5] Rene Gerritsma, Gerhard Kirchmair, Florian Zähringer, E. Solano, R. Blatt, and C. F. Roos, Quantum simulation of the dirac equation, Nature **463**, 68 (2010).

[6] Jacob Biamonte, Peter Wittek, Nicola Pancotti, Patrick Rebentrost, Nathan Wiebe, and Seth Lloyd, Quantum machine learning, Nature **549**, 195 (2017).

[7] Seth Lloyd, Masoud Mohseni, and Patrick Rebentrost, Quantum algorithms for supervised and unsupervised machine learning, arXiv:1307.0411 (2013).

[8] Vedran Dunjko, Jacob M. Taylor, and Hans J Briegel, Quantum-Enhanced Machine Learning, Phys. Rev. Lett. **117**, 130501 (2016).

[9] Maria Schuld and Nathan Killoran, Quantum Machine Learning in Feature Hilbert Spaces, Phys. Rev. Lett. **122**, 040504 (2019).

[10] Nikolaj Moll, Panagiotis Barkoutsos, Lev S. Bishop, Jerry M. Chow, Andrew Cross, Daniel J. Egger, Stefan Filipp, Andreas Fuhrer, Jay M. Gambetta, Marc Ganzhorn, *et al.*, Quantum optimization using variational algorithms on near-term quantum devices, Quantum Sci. Technol. **3**, 030503 (2018).

[11] Edward Farhi and Aram W. Harrow, Quantum supremacy through the quantum approximate optimization algorithm, arXiv:1602.07674 (2016).

[12] Frank Arute, Kunal Arya, Ryan Babbush, Dave Bacon, Joseph C. Bardin, Rami Barends, Sergio Boixo, Michael Broughton, Bob B. Buckley, David A. Buell, *et al.*, Quantum approximate optimization of non-planar graph problems on a planar superconducting processor, arXiv:2004.04197 (2020).

[13] Nicolas Gisin, Grégoire Ribordy, Wolfgang Tittel, and Hugo Zbinden, Quantum cryptography, Rev. Mod. Phys. **74**, 145 (2002).

[14] Charles H. Bennett and Gilles Brassard, Quantum cryptography: Public key distribution and coin tossing, Theor. Comput. Sci. **560**, 7 (2014).

[15] Frank Arute, Kunal Arya, Ryan Babbush, Dave Bacon, Joseph C. Bardin, Rami Barends, Rupak Biswas, Sergio Boixo, Fernando G.S.L. Brandao, David A. Buell, *et al.*, Quantum supremacy using a programmable superconducting processor, Nature **574**, 505 (2019).

[16] Edward Farhi, Jeffrey Goldstone, Sam Gutmann, Joshua Lapan, Andrew Lundgren, and Daniel Preda, A quantum adiabatic evolution algorithm applied to random instances of an np-complete problem, Science **292**, 472 (2001).

[17] Andris Ambainis and Oded Regev, An elementary proof of the quantum adiabatic theorem, arXiv:quant-ph/0411152 (2004).

[18] A. P. Young, S. Knysh, and V. N. Smelyanskiy, First-Order Phase Transition in the Quantum Adiabatic Algorithm, Phys. Rev. Lett. **104**, 020502 (2010).

[19] Xinhua Peng, Zeyang Liao, Nanyang Xu, Gan Qin, Xianyi Zhou, Dieter Suter, and Jiangfeng Du, Quantum Adiabatic Algorithm for Factorization and its Experimental Implementation, Phys. Rev. Lett. **101**, 220405 (2008).

[20] Ben W. Reichardt, in *Proceedings of the thirty-sixth annual ACM symposium on Theory of computing* (Association for Computing Machinery, 2004), p. 502–510.

[21] Matthias Steffen, Wim van Dam, Tad Hogg, Greg Breyta, and Isaac Chuang, Experimental Implementation of an Adiabatic Quantum Optimization Algorithm, Phys. Rev. Lett. **90**, 067903 (2003).

[22] Victor Bapst, Laura Foini, Florent Krzakala, Guilhem Semerjian, and Francesco Zamponi, The quantum adiabatic algorithm applied to random optimization problems: The quantum spin glass perspective, Phys. Rep. **523**, 127 (2013).

[23] Arnab Das and Bikas K. Chakrabarti, Colloquium: Quantum annealing and analog quantum computation, Rev. Mod. Phys. **80**, 1061 (2008).

[24] Mark W. Johnson, Mohammad H. S. Amin, Suzanne Gildert, Trevor Lanting, Firas Hamze, Neil Dickson, Richard Harris, Andrew J Berkley, Jan Johansson, Paul Bunyk, *et al.*, Quantum annealing with manufactured spins, Nature **473**, 194 (2011).

[25] Sergio Boixo, Tameem Albash, Federico M. Spedalieri, Nicholas Chancellor, and Daniel A. Lidar, Experimental signature of programmable quantum annealing, Nat. Commun. **4**, 1 (2013).

[26] Dorit Aharonov, Wim Van Dam, Julia Kempe, Zeph Landau, Seth Lloyd, and Oded Regev, Adiabatic quantum computation is equivalent to standard quantum computation, SIAM Rev. **50**, 755 (2008).

[27] Rami Barends, Alireza Shabani, Lucas Lamata, Julian Kelly, Antonio Mezzacapo, Urtzi Las Heras, Ryan Babbush, Austin G. Fowler, Brooks Campbell, Yu Chen, *et al.*, Digitized adiabatic quantum computing with a superconducting circuit, Nature **534**, 222 (2016).

[28] Erik Torrontegui, Sara Ibáñez, Sofia Martínez-Garaot, Michele Modugno, Adolfo del Campo, David Guéry-Odelin, Andreas Ruschhaupt, Xi Chen, and Juan Gonzalo Muga, Shortcuts to adiabaticity, Adv. At. Mol. Opt. Phys. **62**, 117 (2013).

[29] D. Guéry-Odelin, A. Ruschhaupt, A. Kiely, E. Torrontegui, S. Martínez-Garaot, and J. G. Muga, Shortcuts to adiabaticity: Concepts, methods, and applications, Rev. Mod. Phys. **91**, 045001 (2019).

[30] Kazutaka Takahashi, Hamiltonian engineering for adiabatic quantum computation: Lessons from shortcuts to adiabaticity, J. Phys. Soc. Jpn. **88**, 061002 (2019).

[31] Mustafa Demirplak and Stuart A. Rice, Adiabatic population transfer with control fields, J. Phys. Chem. A **107**, 9937 (2003).

[32] Mustafa Demirplak and Stuart A. Rice, Assisted adiabatic passage revisited, J. Phys. Chem. B **109**, 6838 (2005).

[33] M. V. Berry, Transitionless quantum driving, J. Phys. A: Math. Theor. **42**, 365303 (2009).

[34] Xi Chen, A. Ruschhaupt, S. Schmidt, A. del Campo, D. Guéry-Odelin, and J. G. Muga, Fast Optimal Frictionless Atom Cooling in Harmonic Traps: Shortcut to Adiabaticity, Phys. Rev. Lett. **104**, 063002 (2010).

[35] Xi Chen, E. Torrontegui, and J. G. Muga, Lewis-riesenfeld invariants and transitionless quantum driving, Phys. Rev. A **83**, 062116 (2011).

[36] Shumpei Masuda and Katsuhiro Nakamura, Fast-forward problem in quantum mechanics, Phys. Rev. A **78**, 062108 (2008).

[37] Shumpei Masuda and Katsuhiro Nakamura, Fast-forward of adiabatic dynamics in quantum mechanics, Proc. R. Soc. Lond. A: Math. Phys. Eng. Sci. **466**, 1135 (2010).

[38] Jean-François Schaff, Xiao-Li Song, Patrizia Vignolo, and Guillaume Labeyrie, Fast optimal transition between two equilibrium states, Phys. Rev. A **82**, 033430 (2010).

[39] Shuoming An, Dingshun Lv, Adolfo Del Campo, and Kihwan Kim, Shortcuts to adiabaticity by counterdiabatic driving for trapped-ion displacement in phase space, Nat. Commun. **7**, 12999 (2016).

[40] Yan-Xiong Du, Zhen-Tao Liang, Yi-Chao Li, Xian-Xian Yue, Qing-Xian Lv, Wei Huang, Xi Chen, Hui Yan, and Shi-Liang Zhu, Experimental realization of stimulated raman shortcut-to-adiabatic passage with cold atoms, Nat. Commun. **7**, 1 (2016).

[41] Andrew Lucas, Ising formulations of many np problems, Front. Phys. **2**, 5 (2014).

[42] Adolfo del Campo, Marek M. Rams, and Wojciech H. Zurek, Assisted Finite-Rate Adiabatic Passage across a Quantum Critical Point: Exact Solution for the Quantum Ising Model, Phys. Rev. Lett. **109**, 115703 (2012).

[43] A. Barış Özgüler, Robert Joynt, and Maxim G. Vavilov, Steering random spin systems to speed up the quantum adiabatic algorithm, Phys. Rev. A **98**, 062311 (2018).

[44] Kazutaka Takahashi, Transitionless quantum driving for spin systems, Phys. Rev. E **87**, 062117 (2013).

[45] Andreas Hartmann and Wolfgang Lechner, Rapid counter-diabatic sweeps in lattice gauge adiabatic quantum computing, New J. Phys. **21**, 043025 (2019).

[46] Francesco Petiziol, Benjamin Dive, Florian Mintert, and Sandro Wimberger, Fast adiabatic evolution by oscillating initial Hamiltonians, Phys. Rev. A **98**, 043436 (2018).

[47] Tomáš Opatrnỳ and Klaus Mølmer, Partial suppression of nonadiabatic transitions, New J. Phys. **16**, 015025 (2014).

[48] Francesco Petiziol, Benjamin Dive, Stefano Carretta, Riccardo Mannella, Florian Mintert, and Sandro Wimberger, Accelerating adiabatic protocols for entangling two qubits in circuit qed, Phys. Rev. A **99**, 042315 (2019).

[49] Yunlan Ji, Ji Bian, Xi Chen, Jun Li, Xinfang Nie, Hui Zhou, and Xinhua Peng, Experimental preparation of Greenberger–Horne–Zeilinger states in an Ising spin model by partially suppressing the nonadiabatic transitions, Phys. Rev. A **99**, 032323 (2019).

[50] Hui Zhou, Yunlan Ji, Xinfang Nie, Xiaodong Yang, Xi Chen, Ji Bian, and Xinhua Peng, Experimental Realization of Shortcuts to Adiabaticity in a Nonintegrable Spin Chain by Local Counterdiabatic Driving, Phys. Rev. Appl. **13**, 044059 (2020).

[51] Walter Vinci and Daniel A. Lidar, Non-stoquastic Hamiltonians in quantum annealing via geometric phases, npj Quantum Inf. **3**, 1 (2017).

[52] Kazutaka Takahashi, Shortcuts to adiabaticity for quantum annealing, Phys. Rev. A **95**, 012309 (2017).

[53] G. Passarelli, V. Cataudella, R. Fazio, and P. Lucignano, Counterdiabatic driving in the quantum annealing of the p-spin model: A variational approach, Phys. Rev. Res. **2**, 013283 (2020).

[54] Steve Campbell, Gabriele De Chiara, Mauro Paternostro, G. Massimo Palma, and Rosario Fazio, Shortcut to Adiabaticity in the Lipkin–Meshkov–Glick Model, Phys. Rev. Lett. **114**, 177206 (2015).

[55] Hamed Saberi, Tomáš Opatrnỳ, Klaus Mølmer, and Adolfo del Campo, Adiabatic tracking of quantum many-body dynamics, Phys. Rev. A **90**, 060301 (2014).

[56] C. Whitty, A. Kiely, and A. Ruschhaupt, Quantum control via enhanced shortcuts to adiabaticity, Phys. Rev. Res. **2**, 023360 (2020).

[57] Dries Sels and Anatoli Polkovnikov, Minimizing irreversible losses in quantum systems by local counterdiabatic driving, Proc. Nat. Acad. Sci. **114**, E3909 (2017).

[58] Pieter W. Claeys, Mohit Pandey, Dries Sels, and Anatoli Polkovnikov, Floquet-Engineering Counterdiabatic Protocols in Quantum Many-Body Systems, Phys. Rev. Lett. **123**, 090602 (2019).

[59] Lukas M. Sieberer, Tobias Olsacher, Andreas Elben, Markus Heyl, Philipp Hauke, Fritz Haake, and Peter Zoller, Digital quantum simulation, trotter errors, and quantum chaos of the kicked top, npj Quantum Inf. **5**, 1 (2019).

[60] Masuo Suzuki, Generalized Trotter's formula and systematic approximants of exponential operators and inner derivations with applications to many-body problems, Commun. Math. Phys. **51**, 183 (1976).

[61] Ibm quantum experience, https://www.research.ibm.com/ibm-q/.

[62] Takuya Hatomura, Shortcuts to adiabaticity in the infinite-range Ising model by mean-field counter-diabatic driving, J. Phys. Soc. Jpn. **86**, 094002 (2017).

[63] Michael Kolodrubetz, Dries Sels, Pankaj Mehta, and Anatoli Polkovnikov, Geometry and non-adiabatic response in quantum and classical systems, Phys. Rep. **697**, 1 (2017).

[64] Steve Campbell and Sebastian Deffner, Trade-Off between Speed and Cost in Shortcuts to Adiabaticity, Phys. Rev. Lett. **118**, 100601 (2017).

[65] Yuanjian Zheng, Steve Campbell, Gabriele De Chiara, and Dario Poletti, Cost of counterdiabatic driving and work output, Phys. Rev. A **94**, 042132 (2016).

[66] Obinna Abah, Ricardo Puebla, Anthony Kiely, Gabriele De Chiara, Mauro Paternostro, and Steve Campbell, Energetic cost of quantum control protocols, New J. Phys. **21**, 103048 (2019).

[67] Jarrod R. McClean, Jonathan Romero, Ryan Babbush, and Alán Aspuru-Guzik, The theory of variational hybrid quantum-classical algorithms, New J. Phys. **18**, 023023 (2016).

[68] Edward Farhi, Jeffrey Goldstone, and Sam Gutmann, A quantum approximate optimization algorithm, arXiv:1411.4028 (2014).

[69] Yongcheng Ding, Yue Ban, José D. Martín-Guerrero, Enrique Solano, Jorge Casanova, and Xi Chen, Breaking adiabatic quantum control with deep learning, arXiv:2009.04297 (2020).

[70] Jiahao Yao, Lin Lin, and Marin Bukov, Reinforcement learning for many-body ground state preparation based on counter-diabatic driving, arXiv:2010.03655 (2020).

[71] Gianluca Passarelli, Vittorio Cataudella, Rosario Fazio, and Procolo Lucignano, Counterdiabatic driving in the quantum annealing of the p-spin model: A variational approach, Phys. Rev. Res. **2**, 013283 (2020).

[72] Naomichi Hatano and Masuo Suzuki, in *Quantum annealing and other optimization methods* (Springer, Berlin, Heidelberg, 2005), pp. 37–68.

[73] David Poulin, Angie Qarry, Rolando Somma, and Frank Verstraete, Quantum Simulation of Time-Dependent Hamiltonians and the Convenient Illusion of Hilbert Space, Phys. Rev. Lett. **106**, 170501 (2011).

[74] Christopher M. Dawson and Michael A. Nielsen, The Solovay–Kitaev algorithm, arXiv:quant-ph/0505030 (2005).

[75] Qiskit: An open-source framework for quantum computing, https://qiskit.org/.

[76] Filip B. Maciejewski, Zoltán Zimborás, and Michał Oszmaniec, Mitigation of readout noise in near-term quantum devices by classical post-processing based on detector tomography, Quantum **4**, 257 (2020).